PROCEEDINGS OF SCIENCE

Gravitational Waves from the innermost parts of Core-Collapse Supernovae

Pia Jakobus,[a,b,*] **Bernhard Müller,**[b] **and Alexander Heger**[b]

[a] *University of Hamburg,*
Hamburger Sternwarte, Gojenbergsweg 112, 21029, Hamburg, Germany
[b] *School of Physics and Astronomy, Monash University,*
VIC 3800, Australia
E-mail: pia.jakobus@uni-hamburg.de, bernhard.mueller@monash.edu, alexander.heger@monash.edu

Gravitational waves (GWs) from core-collapse supernovae (CCSNe) could offer a direct probe of the dense core of a proto-compact star (PCS), in which matter can reach densities of multiple times nuclear saturation density. We present axisymmetric simulations of CCSNe using two different models for the high-energy equations of state (EoS), the purely hadronic SFHx model and the CMF model with a smooth crossover to quark matter. We identify a distinct GW signature from a quadrupolar ${}^2g_1$-mode located in the PCS core. This mode is excited by PCS convection, and its frequency strongly depends on the EoS. We attribute the lower mode frequency to the stiffer CMF EoS and its higher sound speed at about twice nuclear saturation density, ρ_0. We summarize our semi-analytic expression that connects the mode frequency to PCS bulk parameters such as its mass, radius, and entropy profile, along with an EoS-dependent factor.

The XVIth Quark Confinement and the Hadron Spectrum Conference (QCHSC24)
19-24 August, 2024
Cairns Convention Centre, Cairns, Queensland, Australia

*Speaker

 ISSN 1824-8039 . Published by SISSA Medialab.

PoS(QCHSC24)227

1. Introduction

Detecting gravitational waves (GWs) from a galactic or nearby core-collapse supernova (CCSN) would be a Rosetta Stone of modern multi-messenger astrophysics, completing the "triad" of CCSN signals alongside neutrino signatures and electromagnetic radiation.

Most of the energy liberated during core-collapse is later, on timescales of seconds, radiated away via neutrino emission [1, 2]. Due to their weakly interacting nature, neutrinos are notoriously difficult to detect. Given their prolific output as "neutrino factories", CCSN, among all astrophysical transients, unsurprisingly remain the most promising candidates for future detections. Only a few tens of low-energy neutrinos had been detected in the famous, SN 1987A, located "nearby" at about 50 kpc from Earth, in the Large Magellanic Cloud [3–5]. Despite the low detection count of this so far unique neutrino detection event from a CCSN, the total count, energy, and timing of the detected neutrinos from SN 1987A still helped us validate fundamental theoretical predictions about the compact remnant [6–10]. Next generation neutrino detectors such as Hyper-Kamiokande will reach as far as Andromeda (~750 kpc from Earth) [11]. Thanks to wide-field transient surveys, *electromagnetic observations* of CCSNe have become frequent[1]. Approximately 10 000 events per year are captured, with detectable distances up to hundreds of Mpc[2] [12]. This number is expected to grow substantially with the Vera C. Rubin Observatory [13].

Whereas EM emission is primarily emitted from the outer ejecta of the star and interacts strongly with matter, and neutrinos decouple from regions near the surface of the proto-compact star (PCS), *GWs* uniquely provide a direct (and unimpeded) probe of the *innermost regions* of the PCS, where densities exceed several times nuclear saturation density. To observe GWs from a CCSN with current detector sensitivity, the event must occur "close", that is, within tens of kpc from Earth. Explosions with rapid rotation could be detected outside the Milky Way up to 100 kpc for energetic explosions of rapidly-rotating progenitor stars [14] - studies by [15] even find distances up to 130 kpc with current detectors, including rapid rotation and also magnetic fields. Future detectors such as the Einstein Telescope can hopefully observe "canonical CCSNe" even beyond the Large Magellanic Cloud [16–18]. The last recorded Galactic supernova, Kepler's Supernova in 1604, was a Type Ia event, located at a distance of approximately ~6 kpc from Earth [19]. Whereas stochastic in nature, the absence of a galactic supernova in over four centuries is surprising, given the expected Galactic rate of a few per century [20], suggesting that the Milky Way has been very quiescent in recent centuries (or that recent explosions have simply escaped our detection).

Contrary to the GW signal of binary neutron star mergers (BNS), where the chirp-like waveform is rather regular, the GW signal of CCSN is expected to be extremely noisy due to non-linear effects of fluid instabilities. The GW spectrograms from multi-dimensional simulations [e.g., 21–31] allow us to extract distinct GW "bands", that reflect PCS oscillation modes, triggered by convection [21, 22, 25, 28, 30–32], the standing-accretion shock instability (SASI) [33], or triaxial instabilities in rotating models [34–37]. McDermott et al. (1983) were among the first to analytically derive

[1] See for example here https://www.rochesterastronomy.org/supernova.html.
[2] It is expected that one CCSN occurs each *second* in our universe.

oscillatory PCS perturbations with finite internal temperature profile, and proposed the existence of gravity (g-) modes associated with the *surface* of the PCS [38]. G-modes occur in convectively stable regions, with buoyancy acting as the restoring force. The characteristic frequency of these modes scales with the peak Brunt-Väisälä frequency, which kind of represents the maximum acceleration experienced by a fluid element displaced within a stably stratified region. This is ultimately responsible for generating a time-varying mass quadrupole moment.

The most robust and rather well understood feature in the GW signal from multi-D CCSN simulations comes from a quadrupolar f/g-mode [22, 28, 39–43] with a frequency that increases in time from a few hundred Hz to above 1 kHz. Unfortunately, the dominant f/g-mode is largely confined to the PCS surface region and therefore only indirectly sensitive to EoS, through bulk PCS parameters such as its mass, radius, surface temperature [22, 44, 45].

More recently, the ${}^2g_1$-mode in the PCS core has received attention [46]. This core g-mode[3] has been found in previous 2D simulations [44, 47, 48] and also in 3D [32]. In the following, we compare the GW signals from CCSN simulations using two different EoS; the purely hadronic SFHx EoS [49] and the CMF EoS [50] with a smooth crossover to quark matter. We find that the core g-mode signature appears at lower frequencies in the `CMF` model compared to `SFHx`, and we identify the underlying EoS properties responsible for this difference. We also briefly discuss reasons for the decreasing trajectory of the core g-mode frequency, and present a universal fit formula for the mode frequency based on PCS properties such as mass, radius, and entropy profile.

All of the following work is based on [46, 51, 52]. For a more detailed overview, we refer the reader to these publications.

2. Methods

We perform axisymmetric (2D) simulations with the general-relativistic neutrino hydrodynamics code CoCoNuT-FMT [53, 54]. To resolve core oscillations, we calculate only a small inner region of radius < 1380 m in spherical symmetry. GW signals are calculated using a modified version [22] of the time-integrated quadrupole formula [55]. Here, we show a zero-metallicity progenitors 85 $M_\odot$ (named z85), which is calculated with the stellar evolution code Kepler [56, 57], and employ two different high-density EoS. For Model `z85:CMF`, we use the chiral mean field model (CMF) with a first-order nuclear liquid-vapor phase transition at densities ρ_0, a second, but weak first order phase transition due to chiral symmetry restoration at about $\sim 4 \times \rho_0$ with a critical endpoint at T_{CeP} approximately 15 MeV, and a smooth transition to quark matter at higher densities [50]. The second EoS, used for Model `z85:SFHx`, is the purely hadronic relativistic mean-field `SFHx` model [49].

[3] We refer to it as *core*, as it is located in the innermost region of the PCS.

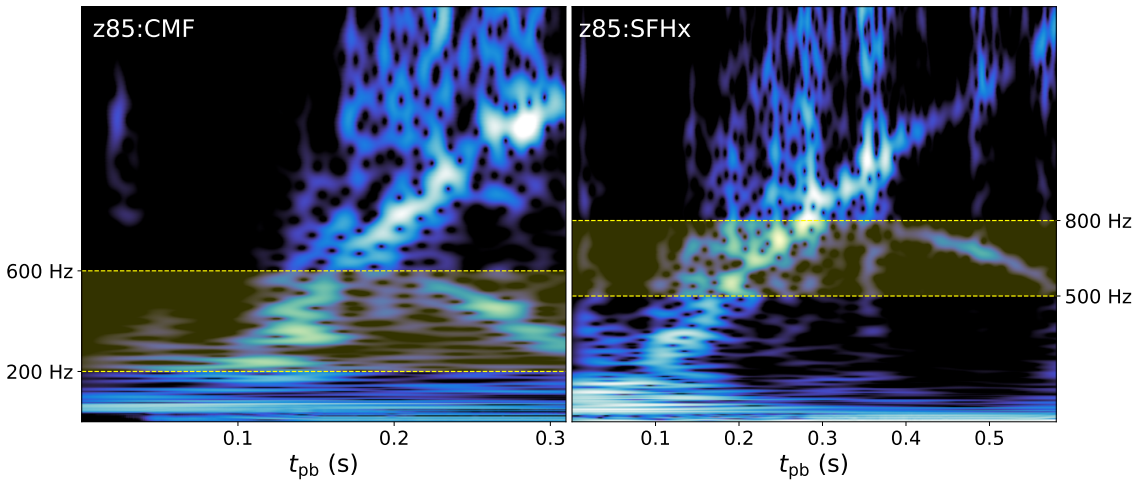

Figure 1: GW spectrograms for `z85:CMF` (left) and `z85:SFHx` (right). The same logarithmic color scale for the amplitude $|h^+|$ (not shown) is used for both models. Both models exhibit the distinct second frequency band (shaded area in yellow) from the ${}^2g_1$-mode, which branches off the dominant band after a few hundred milliseconds. Its frequency depends on the EoS. Data taken from [46], replotted.

3. Results

3.1 The core g-mode in the GW spectrograms

Our axisymmetric simulations show a new feature in the GW spectrograms in Fig. 1, that has so far not been properly identified with respect to its origin [44, 47, 48], or, where the primary trace of the ${}^2g_1$ mode has instead been an emission *gap* at the avoided crossing with the f/g-mode [28]. The GW spectrograms in Fig. 1 are computed using the Morlet wavelet transform and both `CMF` (left side) and `SFHx` (right side) models show distinct differences. While both simulations feature a strong surface f/g-mode band increasing from ~200 Hz to over 1 kHz, both `CMF` models, and Model `z85:SFHx` additionally exhibit a prominent secondary emission band of decreasing frequency, which we will identify as the core ${}^2g_1$-mode. According to linear mode analysis (see [28, 41, 42, 44, 45] for the methodology), this frequency band is the decreasing branch of the ${}^2g_1$ mode, i.e., a quadrupolar g-mode with one node, with an eigenfunction mostly confined to the PCS core region. This core g-mode is notably absent in the `z35:SFHx` model (see [46]) and appears at systematically lower frequencies in `CMF` models compared to `SFHx`[4] models. In Model `z85:CMF`, the ${}^2g_1$ frequency decreases from ~600 Hz to ~220 Hz before black hole formation, compared to ~800 Hz to ~500 Hz for Model `z85:SFHx`.

3.2 Location of the core g-mode

Having preliminarily referred to the new GW feature as the *core* g-mode, we now turn to actually explaining its nomenclature based on its spatial origin. To do so, we perform a spatially resolved Fourier analysis of the integrand of the modified quadrupole formula using high-time-resolution

[4]Model `z35:SFHx` shows equal frequencies to Models `z85:SFHx`, and `z35:CMF` and `z85:CMF` have very similar frequencies, see the more detailed spectrograms for both progenitors in [46].

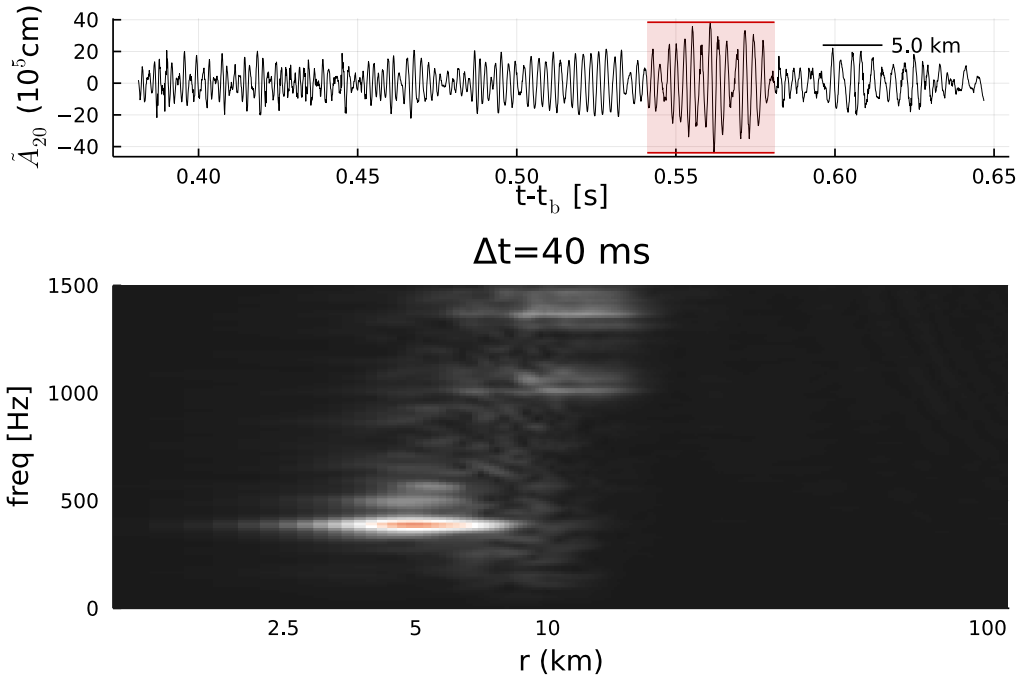

Figure 2: GW amplitude at 5 km (upper panel) and radially resolved GW signal (lower panel) for Model `z35:CMF`. The Fourier transform is computed in a time interval of 40 ms, and indicated in the shaded region in the upper plot. At around 550 ms, the signal strength of this model peaks. Data taken from [46], replotted.

simulation output with sampling frequency 10^4 Hz. To detect quadrupolar motions as a function of radius and frequency, we perform the integral over angle only, and obtain a radius-dependent measure $q(r,t)$ of quadrupolar perturbations, We then obtain spectrograms of $q(r,t)$ using the Fast-Fourier transforms (FFT) in a fixed time window $\Delta t = 40$ ms and apply additional denoising by convolving the FFT with a weighted sum of radial basis functions [58].

We display the GW amplitude and its Fourier transform for Model `z35:CMF` in Fig. 2. The upper panel shows the modified GW amplitude extracted at 5 km as function of post-boune time. The shaded area marks the time interval during which the Fourier transform is computed. The lower panel shows the corresponding radially resolved GW Fourier transform. The signal is located at about 3–10 km.

To give a better view of the location of the core g-mode, we show four different snapshots of the PCS in Fig. 3. Plotted are slices through the polar plane of Model `z85:CMF`, with entropy on the left-hand side of each subplot, and turbulent velocity shown on the right-hand side. We also show the mass coordinate (upper x-axis), time in yellow, overshooting layers (yellow dotted), and g-mode regions (pink hatched). The evolution is shown at four different post-bounce times. Initially, the shock has stalled at around 190 km, with the large-scale SASI present. From about 100 ms post-bounce, the neutrinos streaming from the neutrinosphere become effective at heating the region behind the shock. The inner boundary of the heating region is seen as a sharp entropy step from hot to cool. A zoom into the PCS region ($R \leq 30$ km) shows the PCS, whose radius $R_{\rm PCS}$

is approximately where the neutrinosphere is located. Near this surface region lies the convectively stable surface layer of the PCS, where gravity waves can be excited. These appear as ripples in the non-radial velocity field (shown in grey). The overshooting region, marked as yellow dotted below, is impinged by convection from below, which, together with accretion and the SASI from above, excites the prominent quadrupolar surface f/g-mode, that was seen in Fig. 1. There is a disagreement on the dominant driving mechanism of this surface g-mode in the current literature. Some studies suggest that the primary excitation of the GW signal originates in the PCS convection zone [25, 31], whereas others attribute it to mass accretion down-pinging onto the PCS surface [30, 32]. Further zoomed in (lower right plot), and deeper within the PCS, a second inner core g-mode is located. This mode is primarily excited by convection from the PCS convection zone *above*. The origin of this convective zone is driven by the development of a negative entropy gradient that forms as neutrinos begin to stream of freely from the neutrinosphere, leading to the cooling of the PCS. The resulting negative entropy gradient establishes a convectively unstable stratification (according to the Schwarzschild criterion [59]). This also explains why the core g-mode appears only several hundred milliseconds after core bounce, once neutrinos can escape, which drives the onset of PCS convection. The stable region where the inner core g-mode is located, is in fact a "relict" from the initial shock, which leaves behind a cold, unshocked core and a hot mantle. The corresponding positive entropy profile (cold to hot) is Schwarzschild stable. Of course, convective stability according to the Ledoux criterion [60] is in fact an interplay with also the electron fraction gradient and its thermodynamic pre-factor, however these two derivatives were found to be significantly smaller in our 2D simulations, a behaviour which we also use for our mode approximation. Lastly (lower left), at about 210 ms post-bounce, inverted convection penetrates the innermost PCS region, a phenomenon discussed in [61].

3.3 Core g-mode in the QCD phase diagram and its sensitivity to the speed of sound c_s^2

It is important to note that quark formation is *not* responsible in the `CMF` models for the smaller mode frequency, or the appearance of the mode. The core g-mode, however, appears in a regime where quarks are already abundant in the CMF model, making it particularly interesting as a potential probe of the onset of deconfinement and associated changes in the thermodynamic properties of dense matter (leading to peculiar effects such as inverted convection [61, 62]).

The Brunt-Väisälä frequency sets the scale of the oscillation frequency of gravity waves and can be written in general relativity as [22][5]

$$\omega_{\mathrm{BV}}^2 = \frac{\mathrm{d}\alpha}{\mathrm{d}r}\frac{\alpha}{h\phi^4}\frac{1}{\rho c_s^2}\left\{\left(\frac{\partial P}{\partial s}\right)_{\rho,Y_e}\frac{\mathrm{d}s}{\mathrm{d}r} + \left(\frac{\partial P}{\partial Y_e}\right)_{\rho,s}\frac{\mathrm{d}Y_e}{\mathrm{d}r}\right\}, \tag{1}$$

Here r is the radial coordinate, α is the lapse function, ϕ is the conformal factor, c_s is the sound speed, P is the pressure, s is the specific entropy, Y_e is the electron fraction, and h is the relativistic enthalpy, which is defined in terms of P, the density ρ and the specific internal energy ϵ as $h = 1 + \epsilon + P/\rho$.[6]

[5] The distinction into effective relativistic acceleration and EoS factors will be of use in Section 3.4.

[6] The relativistic expression of h contains the "+1" or representing the rest mass energy per unit mass in natural units where $c = 1$.

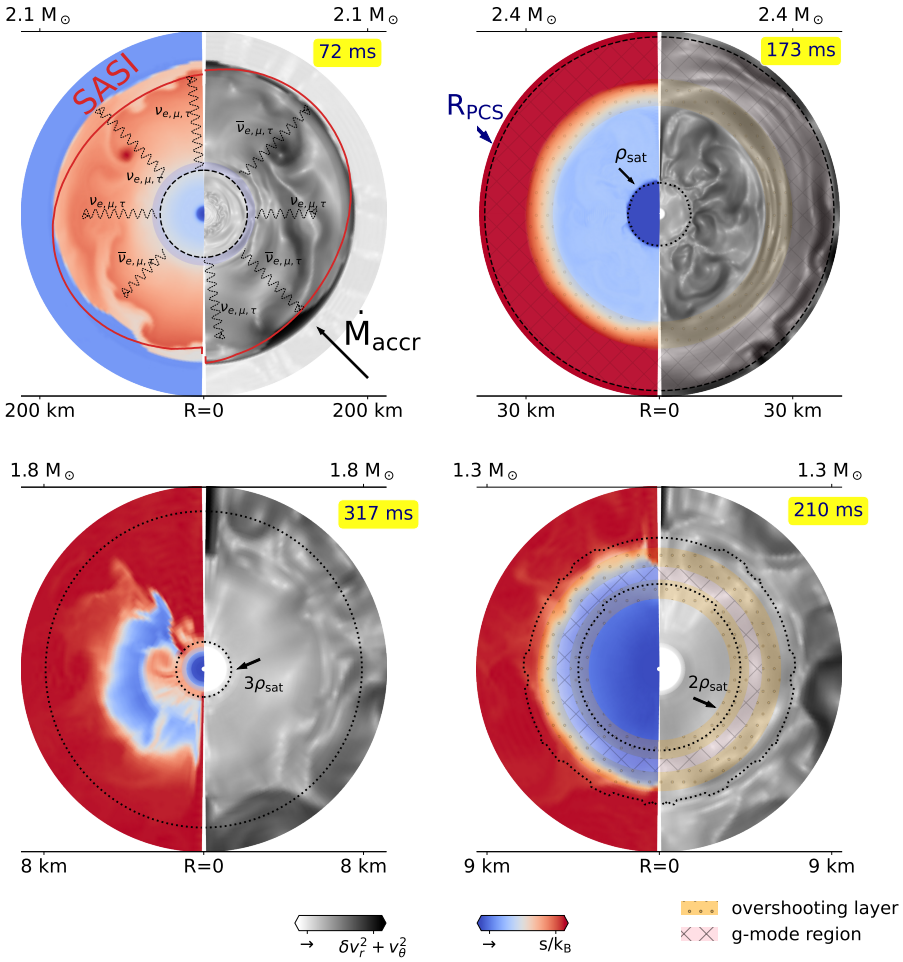

Figure 3: Sketch of the PCS of our `z85:CMF` model, taken from. We show 4 different times going clockwise from upper left to lower left. The left polar plane each shows entropy per baryon s/k_B, the right plane turbulent convective motion. The lower x-axis also displays the radius, while the upper x-axis shows the corresponding enclosed mass. The last snapshot at 317 ms is just before black hole formation. Figure taken from [52].

As mentioned in the previous section, the core g-mode is located at the *inner* boundary of the PCS convection zone, marked by a peak in the Brunt-Väisälä frequency, corresponding to the positive entropy "step" from the initial shock breakout, which acts convectively stabilizing. However, as material overshoots into the g-mode region from *above*, the peak in $\omega^2_{\rm BV}$ becomes smaller, and the entropy profiles flatten (not shown). This flattening behavior of the Brunt-Väisälä frequency $\omega^2_{\rm BV}$ is seen in Fig. 4 by the bell-shaped solid lines, which gradually level out over the course of a few hundred ms. We can trace the GW frequency, by calculating the peak in the Brunt-Väisälä frequency. Notably, the peaks of the Brunt-Väisälä frequency in Fig. 4 are systematically smaller for the `CMF` EoS. Identifying a factor in the Brunt-Väisälä frequency that has lower values in the `CMF` setup due to the thermodynamic properties of the EoS would provide a natural explanation for the lower GW frequencies observed with this EoS compared to `SFHx`. We indeed find, that a higher *sound speed* is

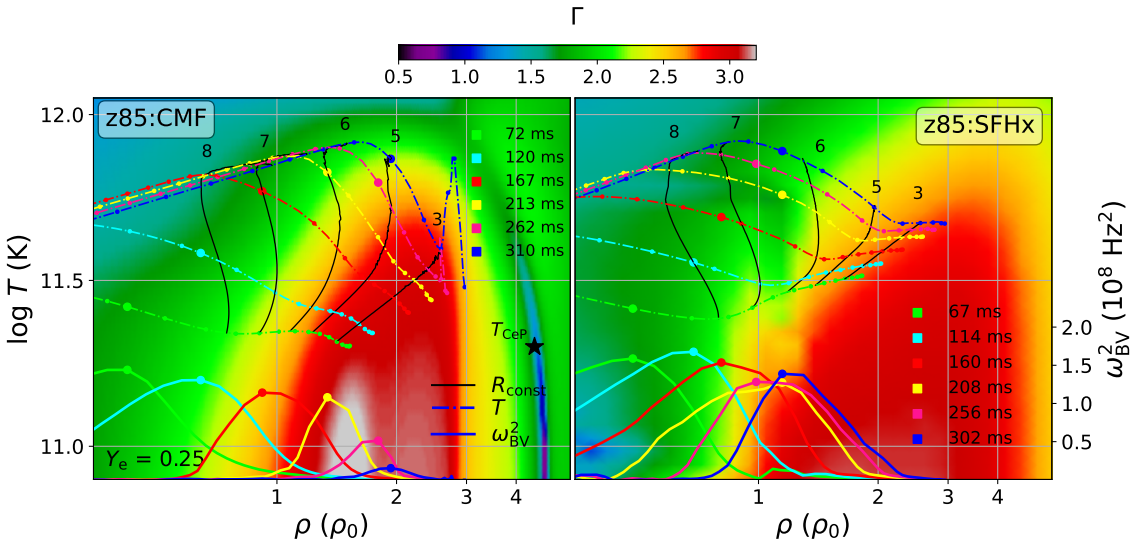

Figure 4: Color contour plots of the adiabatic index Γ as a function of logarithmic temperature T and density in terms of nuclear saturation density ρ/ρ_0 for a constant electron fraction $Y_e = 0.25$ for Models `z85:CMF` (left) and `z35:SFHx` (right). Solid and dashed curves show ω^2_{BV} and temperature profiles $T(\rho)$ (all spherically averaged) at various times (indicated by the line color). The density where ω^2_{BV} peaks is indicated by a dot on the bell-shaped curves. The thin, black lines indicate five constant radii, tracked throughout time, with radius (in km) being indicated on top. Data taken from [46], replotted.

the reason for a smaller Brunt-Väisälä frequency in the `CMF` models, compared to the sound speed in the `SFHx` models, at the location corresponding to the peak value of ω^2_{BV}. The background of Fig. 4 shows the adiabatic index Γ which is closely related to c_s^2 via $\Gamma = \rho c_s^2/P$. Clearly visible is a peak in the adiabatic index at about $\sim 1.3\rho_0$. As the sound speed (and implicitly the adiabatic index times ΓP.[7]) arises in the denominator of Eq. 1, this leads to a smaller Brunt-Väisälä frequency, thus lower GW frequency emission in the CMF runs. The pronounced stiffening of the `CMF` equation of state is due to baryon–baryon repulsion, as discussed in detail by [50]. This stiffening is essential for producing maximum neutron star masses consistent with observational constraints and is already tentatively supported by results from heavy-ion collision experiments [63, 64].

In Fig. 4, we also show the temperature and density evolution of the PCS, and connect points of equal radius by white lines. At 5 km, the temperature drops at about 310 ms, and then increases again at $R \leq 3$ km in Model `z85:CMF`. This occurs because material is transported inward by convection from the hotter, shock-heated outer layers into the cooler core – a process known as inverted convection [61, 62]. Since the SFHx EoS is a purely hadronic EoS, we do not see effects of inverted convection in Model `z85:SFHx`.

3.4 Fitting the core g-mode

If the GW signal from the core g-mode is present and detectable under certain circumstances, we could connect the mode frequency to physical parameters of the PCS and the EoS. In the following,

[7] Because of the factor $1/\rho$ in Eq. 1

we summarize results from [52] for approximating the maximum of $\omega_{\rm BV}$ from Eq. 1 using simple bulk properties of the PCS, such as its mass, radius, and entropy profile at a given fixed mass coordinate, along with an unknown EoS-dependent factor. Ideally, this EoS factor could be inferred by measuring the GW frequency and estimating the PCS bulk parameters entering the approximation.

In the first few hundred ms after bounce, the mass coordinate of the entropy step formed by the early shock propagation remains nearly constant due to efficient neutrino trapping. We can thus approximate the mode location $M_{\rm mode}$, along with the associated entropy and electron fraction gradients, as roughly fixed (this approximation will however break down at later times). The radial profiles of angle-averaged entropy also change little during this early phase, and both the homologous core mass at bounce and the entropy structure near the PCS edge show only weak sensitivity to progenitor differences [65]. Based on our simulations, we therefore choose a constant value of $\mathrm{d}s/\mathrm{d}m \approx 11.93 k_{\rm B}/{\rm M}_\odot$ for the entropy gradient[8]. Furthermore, we neglect the term $(\partial P/\partial Y_{\rm e})_{\rho,s}\,\mathrm{d}Y_{\rm e}/\mathrm{d}r$ as it is about a factor ~12 smaller than the first term in Eq. 1, that is, $(\partial P/\partial s)_{\rho,Y_{\rm e}}\,\mathrm{d}s/\mathrm{d}r$ (during our the time interval of interest). Since the goal is to infer properties about the EoS through our mode approximation, we do not approximate $c_{\rm s}$ and $(\partial P/\partial s)^{1/2}_{\rho,Y_{\rm e}}$. A detailed calculation for the approximation of the metric terms is shown in the Appendix A of [51]. Here, we only quote the result for our final mode relation fit, given by[9]

$$\tilde{\omega}_{\rm BV}^{\rm approx,fix} \approx 0.55 \times \sqrt{\frac{1}{\pi} G M_{\rm mode} \alpha^5_{\rm approx} \frac{1}{c_{\rm s}^2} \left(\frac{\partial P}{\partial s}\right)_{\rho,Y_{\rm e}}} \times 11.93\ k_{\rm B}/{\rm M}_\odot, \tag{2}$$

where we used an additional dimensionless calibration factor $c_{\rm calib} = 0.55$. Furthermore, we chose a fixed mass coordinate of $M_{\rm mode} = 0.72\,{\rm M}_\odot$ for both EoS. The lapse function α is approximated by $\alpha = 1 - Gc^{-2}\,[M_{\rm mode}/r_{\rm mode} - (M_{\rm NS} - M_{\rm mode})/\langle r\rangle]$, with the "effective radius" $\langle r\rangle \equiv c_{\rm eff}(R_{\rm NS} + R_{\rm mode})$.

In Fig. 5, we show results for Models `z85:CMF` and `z85:SFHx`. The correct Brunt-Väisälä frequency from the simulation data at the maximum peak is overlaid onto the spectrograms in red, and the approximations at fixed mass shell are overlaid in dashed-blue. Since the mass coordinate of the core g-mode shifts towards lower values as function of time, the mode is *overestimated* at later times (see blue arrow for CMF). The overestimation of up to 300 Hz is much more pronounced in Model `z85:CMF` because the core g-mode mass coordinate contracts faster in the CMF models. Another error source stems from the entropy gradient approximation $\mathrm{d}s/\mathrm{d}m = \text{const}$, shown in the last panel. Penetration of material into the core g-mode region at later times, and neutrino diffusion ("cooling") together flatten the gradient $\mathrm{d}s/\mathrm{d}m$. The GW frequencies of the mode are quite well tracked by the correct Brunt-Väisälä frequency frequency (red), especially in Model `z85:CMF`, however, it is slightly underestimating the core g-mode in Model `z85:SFHx`. This is only reflecting our choice for the calibration factor though – the trend can be reversed by choosing a slightly increased $c_{\rm calib}$. Still, it is puzzling, why the calibration factor alone cannot align the mode frequencies in the spectrograms of both EoS with $c_{\rm calib}\omega_{\rm BV}^{\rm max}/(2\pi)$.

[8] Rather than directly using the radial entropy gradient, we rewrite $\mathrm{d}s/\mathrm{d}r$ in terms of mass coordinate as $4\pi r^2 \mathrm{d}s/\mathrm{d}m$.
[9] Note, that in the legend of Fig. 5 we use the notation $\tilde{\omega}_{\rm BV} \equiv \omega_{\rm BV}/(2\pi)$.

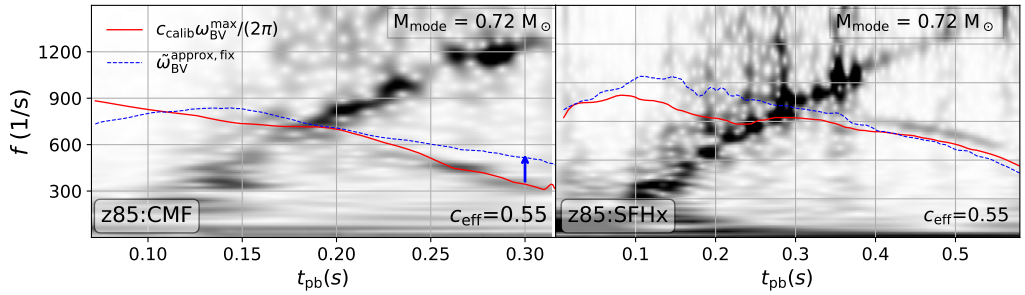

Figure 5: Spectrograms from Fig. 1, overlaid with mode fits for the 2D models Model `z85:CMF` (left), and Model `z85:SFHx` (right). Red lines correspond to the correct Brunt-Väisälä frequency $\omega_{\rm BV}^{\rm max}$, multiplied by a factor $c_{\rm calib}/(2\pi)$. Blue dashed lines show our frequency approximation $\tilde{\omega}_{\rm BV}^{\rm approx,fix}$, following Eq. 2. The fits are evaluated at a fixed mass coordinate $M_{\rm mode} = 0.72 M_\odot$. Data taken from [51], replotted.

The decrease in frequency of the core g-mode is mostly driven by the lapse function α (see Fig. 2 in [51]) which is decreasing as a function of time.[10] Aiding to this effect, the angle-averaged speed of sound profile becomes slightly flatter over time, and $\mathrm{d}s/\mathrm{d}m$ furthermore decreases by neutrino diffusion, and mixing. All in all, this leads to a *decreasing* ${}^2g_1$ mode frequency as function of time.

4. Summary

We have investigated GW signatures from CCSNe as probes of the high-energy equation of state. Using axisymmetric simulations with the CoCoNuT-FMT code and two different high-density EoS models (SFHx and CMF), we identified a distinct GW feature associated with the core ${}^2g_1$-mode, excited by PCS convection. This core g-mode produces a characteristic GW signal with a frequency that decreases in time and is sensitive to the underlying microphysics. In particular, the CMF model exhibits a lower mode frequency due to a stiffer EoS due to a higher sound speed near the convective boundary at multiple times saturation density, where quarks are already present. We derived a semi-analytic fit for the core g-mode frequency based on PCS bulk properties such as mass, radius, and entropy gradient, and traced its evolution over time. Whereas our approximation is only a first step, and improvements are necessary, the idea is to link GW observations to thermodynamic properties of the EoS, where quark matter is present. Finding a way to approximately track the mass shell of the core g-mode, along with a simple fit to estimate the time-dependent $\mathrm{d}s/\mathrm{d}m$, would improve our fit and avoid overestimating the mode frequency at later times. Our work highlights the potential of GWs from CCSNe as a unique laboratory for constraining the high-density EoS. Further simulations are needed to study when and how strongly modes other than the f/g-mode or the SASI are excited and detectable in GWs.

[10] By contrast, the PCS surface f/g mode frequency (which increases as function of time) is proportional to the surface gravity $M_{\rm mode}/r_{\rm mode}^2$.

References

[1] S.A. Colgate and R.H. White, *The Hydrodynamic Behavior of Supernovae Explosions*, *ApJ* **143** (1966) 626.

[2] H.A. Bethe and J.R. Wilson, *Revival of a stalled supernova shock by neutrino heating*, *ApJ* **295** (1985) 14.

[3] K. Hirata, T. Kajita, M. Koshiba, M. Nakahata, Y. Oyama, N. Sato et al., *Observation of a neutrino burst from supernova 1987A.*, in *Neutrino Masses and Neutrino Astrophysics (Including Supernova 1987a)*, V. Barger, F. Halzen, M. Marshak and K. Olive, eds., pp. 51–62, Jan., 1987.

[4] R.M. Bionta, G. Blewitt, C.B. Bratton, D. Casper, A. Ciocio, R. Claus et al., *Observation of a neutrino burst in coincidence with supernova 1987a in the large magellanic cloud*, *Phys. Rev. Lett.* **58** (1987) 1494.

[5] E. Alexeyev, L. Alexeyeva, I. Krivosheina and V. Volchenko, *Detection of the neutrino signal from sn 1987a in the lmc using the inr baksan underground scintillation telescope*, *Physics Letters B* **205** (1988) 209.

[6] B. Müller, *Neutrino emission as diagnostics of core-collapse supernovae*, *Annual Review of Nuclear and Particle Science* **69** (2019) 253.

[7] S.W. Bruenn, *Neutrinos from sn1987a and current models of stellar-core collapse*, *Phys. Rev. Lett.* **59** (1987) 938.

[8] J. Bahcall, T. Piran, W. Press and D. Spergel, *Neutrino temperatures and fluxes from the lmc supernova*, *Nature* **327** (1987) 682.

[9] A. Burrows, *Supernova neutrinos.*, in *Extra Solar Neutrino Astronomy*, D. Cline, ed., pp. 3–8, Jan., 1988.

[10] W.D. Arnett, J.N. Bahcall, R.P. Kirshner and S.E. Woosley, *Supernova 1987A.*, *Annual Review of Astron and Astrophysics* **27** (1989) 629.

[11] K. Scholberg, *Supernova neutrino detection*, in *Journal of Physics Conference Series*, vol. 375 of *Journal of Physics Conference Series*, p. 042036, IOP, July, 2012, DOI.

[12] A. Jerkstrand, D. Milisavljevic and B. Müller, *Core-collapse supernovae*, *arXiv e-prints* (2025) arXiv:2503.01321 [2503.01321].

[13] K.M. Hambleton, F.B. Bianco, R. Street, K. Bell, D. Buckley, M. Graham et al., *Rubin Observatory LSST Transients and Variable Stars Roadmap*, PASP **135** (2023) 105002 [2208.04499].

[14] M.J. Szczepańczyk, J.M. Antelis, M. Benjamin, M. Cavaglià, D. Gondek-Rosińska, T. Hansen et al., *Detecting and reconstructing gravitational waves from the next galactic core-collapse supernova in the advanced detector era*, *Phys. Rev. D* **104** (2021) 102002.

PoS(QCHSC24)227

[15] J. Powell and B. Müller, *The gravitational-wave emission from the explosion of a 15 solar mass star with rotation and magnetic fields*, *Monthly Notices of the Royal Astronomical Society* **532** (2024) 4326 [https://academic.oup.com/mnras/article-pdf/532/4/4326/58713230/stae1731.pdf].

[16] M. Punturo, M. Abernathy, F. Acernese, B. Allen, N. Andersson, Arun et al., *The Einstein Telescope: a third-generation gravitational wave observatory*, *Classical and Quantum Gravity* **27** (2010) 194002.

[17] M. Szczepańczyk and M. Zanolin, *Gravitational Waves from a Core-Collapse Supernova: Perspectives with Detectors in the Late 2020s and Early 2030s*, *Galaxies* **10** (2022) 70.

[18] J. Powell and B. Müller, *Gravitational wave emission from 3D explosion models of core-collapse supernovae with low and normal explosion energies*, *Monthly Notices of the Royal Astronomical Society* **487** (2019) 1178.

[19] D.J. Patnaude, C. Badenes, S. Park and J.M. Laming, *The origin of kepler's supernova remnant*, *The Astrophysical Journal* **756** (2012) 6.

[20] K. Rozwadowska, F. Vissani and E. Cappellaro, *On the rate of core collapse supernovae in the milky way*, *New Astronomy* **83** (2021) 101498 [2009.03438].

[21] J.W. Murphy, C.D. Ott and A. Burrows, *A Model for Gravitational Wave Emission from Neutrino-Driven Core-Collapse Supernovae*, ApJ **707** (2009) 1173.

[22] B. Müller, H.-T. Janka and A. Marek, *A New Multi-dimensional General Relativistic Neutrino Hydrodynamics Code of Core-collapse Supernovae. III. Gravitational Wave Signals from Supernova Explosion Models*, ApJ **766** (2013) 43.

[23] T. Kuroda, T. Takiwaki and K. Kotake, *Gravitational wave signatures from low-mode spiral instabilities in rapidly rotating supernova cores*, Phys. Rev. D **89** (2014) 044011.

[24] T. Kuroda, K. Kotake and T. Takiwaki, *A New Gravitational-wave Signature from Standing Accretion Shock Instability in Supernovae*, *Astrophysical Journal Letters* **829** (2016) L14.

[25] H. Andresen, B. Müller, E. Müller and H.T. Janka, *Gravitational wave signals from 3D neutrino hydrodynamics simulations of core-collapse supernovae*, *Monthly Notices of the Royal Astronomical Society* **468** (2017) 2032.

[26] K.N. Yakunin, A. Mezzacappa, P. Marronetti, E.J. Lentz, Bruenn et al., *The Gravitational Wave Signal of a Core Collapse Supernova Explosion of a 15$M_\odot$ Star*, *arXiv e-prints* (2017) arXiv:1701.07325 [1701.07325].

[27] T. Takiwaki and K. Kotake, *Anisotropic emission of neutrino and gravitational-wave signals from rapidly rotating core-collapse supernovae*, *Monthly Notices of the Royal Astronomical Society* **475** (2018) L91.

[28] V. Morozova, D. Radice, A. Burrows and D. Vartanyan, *The gravitational wave signal from core-collapse supernovae*, *The Astrophysical Journal* **861** (2018) 10.

[29] H. Andresen, E. Müller, H.T. Janka, A. Summa, K. Gill and M. Zanolin, *Gravitational waves from 3D core-collapse supernova models: The impact of moderate progenitor rotation*, *Monthly Notices of the Royal Astronomical Society* **486** (2019) 2238.

[30] D. Radice, V. Morozova, A. Burrows, D. Vartanyan and H. Nagakura, *Characterizing the gravitational wave signal from core-collapse supernovae*, *The Astrophysical Journal Letters* **876** (2019) L9.

[31] A. Mezzacappa, P. Marronetti, R.E. Landfield, E.J. Lentz, K.N. Yakunin, Bruenn et al., *Gravitational-wave signal of a core-collapse supernova explosion of a 15 $M_\odot$ star*, *Phys. Rev. D* **102** (2020) 023027.

[32] D. Vartanyan, A. Burrows, T. Wang, M.S.B. Coleman and C.J. White, *Gravitational-wave signature of core-collapse supernovae*, *Physical Review D* **107** (2023) 103015 [2302.07092].

[33] J.M. Blondin, A. Mezzacappa and C. DeMarino, *Stability of Standing Accretion Shocks, with an Eye toward Core-Collapse Supernovae*, ApJ **584** (2003) 971.

[34] C.D. Ott, H. Dimmelmeier, A. Marek, H.-T. Janka, I. Hawke, B. Zink et al., *3d collapse of rotating stellar iron cores in general relativity including deleptonization and a nuclear equation of state*, *Phys. Rev. Lett.* **98** (2007) 261101.

[35] S. Scheidegger, T. Fischer, S.C. Whitehouse and M. Liebendörfer, *Gravitational waves from 3D MHD core collapse simulations*, *Astronomy and Astrophysics* **490** (2008) 231 [0709.0168].

[36] S. Scheidegger, R. Käppeli, S.C. Whitehouse, T. Fischer and M. Liebendörfer, *The influence of model parameters on the prediction of gravitational wave signals from stellar core collapse*, *Astronomy and Astrophysics* **514** (2010) A51 [1001.1570].

[37] K. Kotake and T. Kuroda, *Gravitational waves from core-collapse supernovae*, in *Handbook of Supernovae*, A.W. Alsabti and P. Murdin, eds., (Cham), pp. 1671–1698, Springer International Publishing (2017), DOI.

[38] P.N. McDermott, H.M. van Horn and J.F. Scholl, *Nonradial g-mode oscillations of warm neutron stars*, *ApJ* **268** (1983) 837.

[39] H. Sotani, T. Kuroda, T. Takiwaki and K. Kotake, *Probing mass-radius relation of protoneutron stars from gravitational-wave asteroseismology*, *Phys. Rev. D* **96** (2017) 063005.

[40] A. Torres-Forné, P. Cerdá-Durán, A. Passamonti and J.A. Font, *Towards asteroseismology of core-collapse supernovae with gravitational-wave observations - I. Cowling approximation*, *MNRAS* **474** (2018) 5272.

[41] A. Torres-Forné, P. Cerdá-Durán, A. Passamonti, M. Obergaulinger and J.A. Font, *Towards asteroseismology of core-collapse supernovae with gravitational wave observations - II.*

Inclusion of space-time perturbations, Monthly Notices of the Royal Astronomical Society **482** (2019) 3967.

[42] O. Eggenberger Andersen, S. Zha, A. da Silva Schneider, A. Betranhandy, S.M. Couch and E.P. O'Connor, *Equation-of-state Dependence of Gravitational Waves in Core-collapse Supernovae*, ApJ **923** (2021) 201.

[43] A. Mezzacappa, P. Marronetti, R.E. Landfield, E.J. Lentz, W.R. Hix, J.A. Harris et al., *Core Collapse Supernova Gravitational Wave Emission for Progenitors of 9.6, 15, and 25 Solar Masses*, *arXiv e-prints* (2022) arXiv:2208.10643 [2208.10643].

[44] A. Torres-Forné, P. Cerdá-Durán, M. Obergaulinger, B. Müller and J.A. Font, *Universal Relations for Gravitational-Wave Asteroseismology of Protoneutron Stars*, Phys. Rev. Lett. **123** (2019) 051102.

[45] H. Sotani, T. Takiwaki and H. Togashi, *Universal relation for supernova gravitational waves*, Phys. Rev. D **104** (2021) 123009.

[46] P. Jakobus, B. Müller, A. Heger, S. Zha, J. Powell, A. Motornenko et al., *Gravitational Waves from a Core g Mode in Supernovae as Probes of the High-Density Equation of State*, Phys. Rev. Lett. **131** (2023) 191201 [2301.06515].

[47] P. Cerdá-Durán, N. DeBrye, M.A. Aloy, J.A. Font and M. Obergaulinger, *Gravitational Wave Signatures in Black Hole Forming Core Collapse*, ApJ **779** (2013) L18.

[48] H. Kawahara, T. Kuroda, T. Takiwaki, K. Hayama and K. Kotake, *A Linear and Quadratic Time-Frequency Analysis of Gravitational Waves from Core-collapse Supernovae*, ApJ **867** (2018) 126.

[49] A.W. Steiner, M. Hempel and T. Fischer, *Core-collapse Supernova Equations of State Based on Neutron Star Observations*, ApJ **774** (2013) 17.

[50] A. Motornenko, J. Steinheimer, V. Vovchenko, S. Schramm and H. Stoecker, *Equation of state for hot qcd and compact stars from a mean-field approach*, *Phys. Rev. C* **101** (2020) 034904.

[51] P. Jakobus, B. Mueller and A. Heger, *Convection and the Core g-mode in Proto-Compact Stars – A detailed analysis*, *arXiv e-prints* (2024) arXiv:2405.01449 [2405.01449].

[52] P. JAKOBUS, *Equation of State effects in Core-Collapse Supernovae*, Ph.D. thesis, 2, 2024. 10.26180/25156541.v1.

[53] B. Müller, H.-T. Janka and H. Dimmelmeier, *A New Multi-dimensional General Relativistic Neutrino Hydrodynamic Code for Core-collapse Supernovae. I. Method and Code Tests in Spherical Symmetry*, ApJS **189** (2010) 104.

[54] B. Müller and H.T. Janka, *Non-radial instabilities and progenitor asphericities in core-collapse supernovae*, MNRAS **448** (2015) 2141.

PoS(QCHSC24)227

[55] L.S. Finn, *Supernovae, gravitational radiation, and the quadrupole formula.*, in *Frontiers in Numerical Relativity*, C.R. Evans, L.S. Finn and D.W. Hobill, eds., pp. 126–145 (1989).

[56] T.A. Weaver, G.B. Zimmerman and S.E. Woosley, *Presupernova evolution of massive stars.*, ApJ **225** (1978) 1021.

[57] A. Heger and S.E. Woosley, *Nucleosynthesis and Evolution of Massive Metal-free Stars*, ApJ **724** (2010) 341.

[58] D.E. Myers, *Smoothing and interpolation with radial basis functions*, *WIT Transactions on Modelling and Simulation* **23** (1970) .

[59] K. Schwarzschild, *Ueber das gleichgewicht der sonnenatmosphäre*, *Nachrichten von der Gesellschaft der Wissenschaften zu Göttingen, Mathematisch-Physikalische Klasse* **1906** (1906) 41.

[60] P. Ledoux, *Stellar Models with Convection and with Discontinuity of the Mean Molecular Weight*, *ApJ* **105** (1947) 305.

[61] P. Jakobus, B. Müller, A. Heger, A. Motornenko, J. Steinheimer and H. Stoecker, *The role of the hadron-quark phase transition in core-collapse supernovae*, *MNRAS* **516** (2022) 2554 [2204.10397].

[62] A.V. Yudin, M. Hempel, D.K. Nadyozhin and T.L. Razinkova, *Some properties of convection in hybrid stars*, *MNRAS* **455** (2016) 4325 [1507.04598].

[63] M. Omana Kuttan, J. Steinheimer, K. Zhou and H. Stoecker, *The QCD EoS of dense nuclear matter from Bayesian analysis of heavy ion collision data*, *arXiv e-prints* (2022) arXiv:2211.11670 [2211.11670].

[64] D. Oliinychenko, A. Sorensen, V. Koch and L. McLerran, *Sensitivity of Au+Au collisions to the symmetric nuclear matter equation of state at 2 – 5 nuclear saturation densities*, 2208.11996.

[65] A. Marek, *Multi-dimensional simulations of core collapse supernovae with different equations of state for hot proto-neutron stars*, Ph.D. thesis, Technische Universität München, 2017.

PoS(QCHSC24)227